Proceedings of ASME Turbo Expo 2012
GT2012
June 11-15, 2012, Copenhagen, Denmark

GT2012-69067

RECENT ADVANCES IN MANUFACTURING OF RIBLETS ON COMPRESSOR BLADES AND THEIR AERODYNAMIC IMPACT

[1]Christoph Lietmeyer, [4]Berend Denkena, [2]Rainer Kling, [4]Thomas Krawczyk, [2]Ludger Overmeyer, [3]Eduard Reithmeier, [3]Renke Scheuer, [3]Taras Vynnyk, [2]Bodo Wojakowski, [1]Joerg R. Seume

[1]Institute of Turbomachinery and Fluid Dynamics
Leibniz Universitaet Hannover
Appelstr.9
30167 Hannover, Germany

[2]Laser Zentrum Hannover e.V.
Hollerithallee 8
30419 Hannover, Germany

[3]Institute of Measurement and Automatic Control
Leibniz Universitaet Hannover
Nienburger Str. 17
30167 Hannover, Germany

[4]Institute of Production Engineering and Machine Tools
Leibniz Universitaet Hannover
An der Universitaet 2
30823 Garbsen, Germany

ABSTRACT

Since Oehlert et al. (2007), significant improvements in the manufacturing processes of riblets by laser-structuring and grinding have been achieved. In the present study, strategies for manufacturing small-scale grooves with a spacing smaller than 40 µm by metal bonded grinding wheels are presented. For the laser-structuring process, significant improvements of the production time by applying diffractive optical elements were achieved. Finally, strategies for evaluating the geometrical quality of the small-scale surface structures are shown and results obtained with two different measuring techniques (SEM and confocal microscope) are compared with each other.

The aerodynamic impact of the different manufacturing processes is investigated based upon skin friction reduction data obtained on flat plates as well as the profile-loss reduction of riblet-structured compressor blades measured in a linear cascade wind tunnel. Numerical simulations with MISES embedded in a Monte Carlo Simulation (MCS) were performed in order to calculate the profile-loss reduction of a blade structured by grinding to define further improvements of the riblet-geometry. A numerical as well as experimental study quantifying the relevant geometrical parameters indicate how further improvements from the present 4 % reduction in skin friction can be achieved by an additional decrease of the riblet tip-diameter and a more trapezoidal shape of the groove in order to realize the 8 % potential reduction.

NOMENCLATURE

A	[µm²]	cross sectional area
a_e	[µm]	cut depth
c	[mm]	chord length
d	[µm]	diameter
d_g	[µm]	grain size
d_{min}	[nm]	limited lateral resolution
d_{wire}	[mm]	diameter of the copper wire
d_0	[µm]	beam distance in focal plane
d_φ	[µm]	beam distance in relation to scanning direction
f_{wire}	[mm]	infeed of the wire
h	[µm]	riblet height
h_{20}	[µm]	profile height at a width of 20 µm
h_{60}	[µm]	profile height at a width of 60 µm
I_{d0}	[A]	short circuit current
L	[mm]	grinding length
M	[-]	Mach number
N	[-]	number of observations
NA	[-]	numerical aperture
p	[Pa]	pressure
r	[µm]	riblet tip-radius
Re	[-]	Reynolds number

s	[µm]	riblet spacing
t	[µm]	riblet tip-diameter
u_τ	[m/s]	(skin) friction velocity
v_c	[m/s]	cutting speed
v_{cd}	[m/s]	cutting speed at dressing
v_{ft}	[mm/min]	feed rate
v_{fwire}	[µm/s]	feed rate of the wire
x, y, z	[mm]	wall coordinates
X	[-]	riblet groove shape factor
$\Delta r_{sw\,r}$	[µm]	radial wheel profile wear
Δz	[mm]	lateral displacement

Greek symbols

α	[°]	flank opening-angle at the riblet tip
φ	[°]	rotation angle
σ	[-]	standard deviation
τ	[N/m²]	wall shear-stress
λ	[nm]	wavelength
ω	[-]	pressure loss coefficient

Subscripts

opt	optimal
tot	total
stat	static
0	reference
+	non-dimensional, in wall coordinates

Abbreviations

DLR	German Aerospace Center
ECDD	Electronic Contact Discharge Dressing
IFW	Institute of Production Engineering and Machine Tools
IMR	Institute for Measurement and Automatic Control
LZH	Laser-Center Hannover
NASA	National Aeronautics and Space Administration
SEM	Scanning Electron Microscope
TFD	Institute of Turbomachinery and Fluid Dynamics

INTRODUCTION

A major goal in turbomachinery design is the increase of efficiency in order to reduce the fuel consumption of aircraft engines or gas turbines and hence the operating costs and CO2-emissions. To attain an increase of efficiency, the flow losses must be reduced. Approximately 50% of the losses are generated by the secondary flows (Gümmer [1]). Thus, approximately 50% of the losses are generated by the blading with a dominant portion of the friction losses, especially in the turbulent boundary layer of compressor blades with an early onset of boundary layer transition near the leading edges. Therefore, a decrease of skin friction leads to an additional increase in efficiency.

It is known that small ribs on the surface, oriented in the mean flow direction, can reduce skin friction in the case of turbulent boundary layer flow when their geometric properties are appropriate to the local flow conditions. These ribs, also known as riblets, are therefore a passive control mechanism to reduce drag and can also be found in nature on the skin of fast swimming sharks (Reif et. al. [2]). The drag reduction mechanism can be related to an interaction of riblets with the streaky structures in the viscous sublayer. Riblets oriented into the mean flow direction can hamper the cross flow of the streak structures at the wall. Hence, the vertical motions of the fluid and the turbulent shear stresses are reduced. The streak structures are moved away from the surface and are primarily in contact with the riblet tips.

Idealized geometries with less complexity in comparison to the shark skin were first investigated on flat plates by Walsh [3] at NASA Langley Research Center. Later, in the 1990's, extensive experimental investigations on the effect of various 2-D riblet geometries on the skin friction of flat plates were carried out by Bechert et al. [4] in the oil channel of the Institute of Propulsion Technology of the German Aerospace Center (DLR) in Berlin. The experiments were confined to flows with zero pressure gradients. The best drag reduction of up to 10% was achieved by blade-type ribs. Unfortunately, the structural strength of this type of geometry is expected to be insufficient under operating conditions of aircraft engines or gas turbines. A good compromise between structural strength and drag-reduction potential is achieved, for instance, by riblets with a trapezoidal or triangular groove.

With these types of riblets, a few experiments were carried out by different research groups in order to investigate their potential to reduce profile losses of compressor blades. A brief overview of the results obtained by different research groups is given in Oehlert and Seume [5]. Most of these investigations involved the application of foils carrying small ribs with ideal groove geometries and sharp tips to the surface of the compressor blades. This application technique is neither suitable for industrial nor aircraft gas turbine engine blading, as the foil is expected to be of insufficient mechanical strength under the operating conditions of these engines.

Ideally, the riblets should be manufactured in the bulk material of the turbine or compressor blade on the same machine tool as is used to machine the airfoil shapes of the blade in order to avoid additional set-up times. This leads to the main objective: The manufacturing of riblets by means of applicable industrial manufacturing processes and is the motivation of the research project "Riblets for compressor blades" funded by the German Research Foundation (DFG).

As shown by Oehlert and Seume [5] and by Oehlert et al. [6], the initial investigations of riblets created on compressor blades by means of industrial manufacturing processes were very promising. The surface structures were produced on the compressor blades by grinding (IFW) and laser-structuring (LZH) as described by Denkena et al. [7] and Siegel et al. [8]. An optimization of the riblet application method by Lietmeyer et al. [9], resulting in an additional reduction of profile loss, involved the adaptation of the riblets to the local flow

conditions and the selective placement of the riblets on the blade surfaces.

The present paper presents recent improvements in grinding and laser-structuring techniques for accurate geometric production of riblets on compressor blades and the reduction of production times. Measuring techniques for the evaluation of the geometry of small scale structures and a methodology for assessing the aerodynamic impact of riblet geometry on compressor blade profile losses are presented finally.

RECENT ADVANCES IN MANUFACTURING OF RIBLETS BY GRINDING

Grinding with multi-profiled wheels has been established as an effective method for generating riblet structures on large-scale surfaces. Vitrified bonded grinding wheels can be used to generate micro groove structures with a width of 26 µm to 120 µm (Figure 1). In order to utilize the full potential of riblet structures with a trapezoidal groove, it is necessary to generate micro profiles with an aspect ratio of riblet height to spacing of $h/s = 0.5$. The ground riblet structures with a spacing of 26 µm, however, did not reach the required aspect ratio and since a riblet spacing as small as 20 µm (with a height of 10 µm) is required for compressor blade applications, the grain size of the abrasive material must be downscaled in order to achieve the required geometries. However, if the grain size is too small, the bonding forces will decrease and the grinding wheel wear will increase (Denkena et al. [7]). In order to reduce tool wear and the dimensional limit inherent in the production of riblet geometries by means of vitrified bonded grinding wheels, metal bonded grinding wheels can be used. Due to the high bonding forces of the metal binding, small grain sizes can be used without an increase of the tool wear (Klocke et al. [10]). In contrast to vitrified bonding, however, metal bonded grinding tools are difficult to dress by conventional dressing methods.

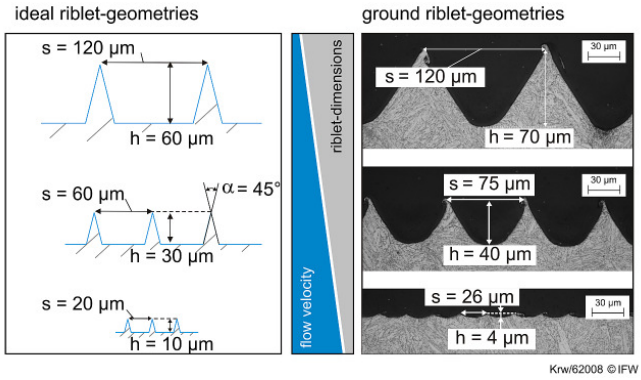

Figure 1: RIBLET GEOMETRIES GROUND BY VITRIFIED BONDED GRINDING WHEELS

In principle, electronic contact discharge dressing (ECDD) is suitable for generating complex profiles on metal bonded wheels (Denkena et al. [11], Zaeh et al. [12]). Here, one pole of the direct current circuit is connected to an electrode and the other pole is connected to the steel body of the grinding tool by carbon brushes. During dressing chips are generated from the electrode, which establish a distortion of the electric field between the electrode and the metal bond. An arc-over is the result of the increasing field distortion and the chip is vaporized. The thermal energy released in this process melts and removes the bond material locally. The dressing strategy is shown in Figure 2. The electrode (a copper wire with a diameter of 1 mm) moves radially to the grinding wheel and generates a trapezoidal groove (Figure 2). In a second step, the wire is displaced about Δz and then moved radially again. Using this strategy, a number of profiles can be created on the grinding wheel. The spacing of the dressed profiles on the grinding wheel is larger than the riblet spacing (Figure 3). However, a riblet spacing smaller than the profiles on the grinding wheel is generated on compressor blades by a shift strategy (Denkena et al. [7]).

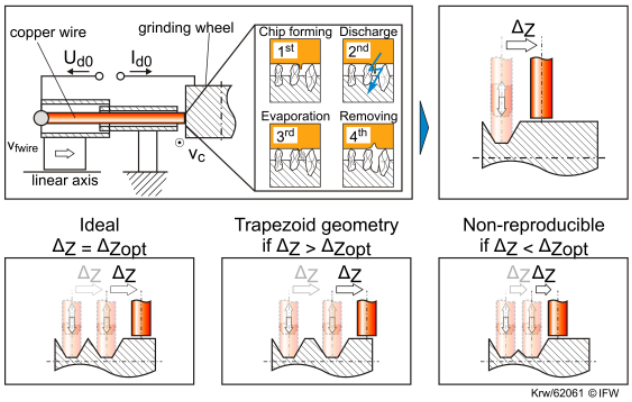

Figure 2: ECDD-STRATEGY

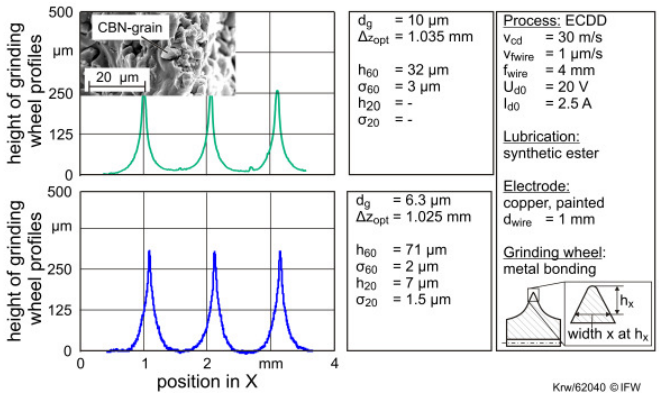

Figure 3: MICRO PROFILES ON THE GRINDING WHEEL

The displacement Δz is varied to find Δz_{opt}, which generates the smallest profile geometries on the grinding wheel. The profile geometries, including the profile heights, are evaluated at a profile width of 20 µm and 60 µm (h_{20} and h_{60}). Trapezoidal profiles will be generated if Δz is too big. In the case of smaller Δz, the height of the micro profiles on the

grinding wheel is reduced by an overlap. This means the smallest profiles will be produced if the dressed geometries just touch each other. In this study grinding wheels (MB6.3 and MB10, Figure 3) with two different grain sizes (6.3 µm and 10 µm) were utilized. The optimal displacement Δz_{opt} for the grinding wheel MB10 was 1.035 µm. The minimum size profiles on grinding wheels with a grain size of 6.3 µm were generated at a Δz_{opt} of 1.025 µm. The displacement Δz_{opt} is dependent on the grain size due to the dressed groove width. During the dressing process, the metal bonding melts, grains fall out and a groove is generated. If a grain with a size of 10 µm falls out, the width of the roof will increase about 10 µm. The increase will be less for smaller grain sizes.

In order to grind riblet structures with a riblet spacing of 20 µm and an aspect ratio of $h/s = 0.5$, the grinding wheel profile should have a height h_{20} of nearly 10 µm. By applying the metal bonded grinding wheel MB10, a profile height of 32 µm was reached at a profile width of 60 µm. A profile height h_{20} could not be measured due to the low sharpness of the profiles. The SEM view shows that there was only one grain on the tip of the grinding wheel profile. As a result, it is not possible to dress smaller profile geometries by applying grinding wheels with a grain size of 10 µm. Compared to the grinding wheel MB10, the profile height h_{60} of the grinding wheel MB6.3 increased about 100% to 72 µm. In addition, both results show that the profile geometries were generated with a high reproducibility (Figure 3). The minimum possible profile geometry is dependent on the grain size due to the fact that at least one grain must be at the peak of the profile. The bigger the grain the bigger the profile geometry. In addition, a great number of grains on the peak of a profile add stability to the peak.

ECDD is a time consuming dressing method. In order to dress grooves with a depth of nearly 250 µm, a copper wire infeed of 4 mm is required. Since the wire moves at a feed rate of 1 µm per second, 264 minutes are required to dress 3 profiles on a grinding wheel. An economical use of metal bonded grinding wheels is possible if the grinding wheels have a low wear rate.

The wear characteristics of metal bonded grinding wheels were thus analyzed as part of the present study. The radial wheel profile wear $\Delta r_{sw\ r}$ was evaluated for different depth of cut a_e and feed rates v_{ft} during the grinding of a typical steel material for compressor blades, X20Cr13 (St1.4021). A nearly linear wear behavior across the grinding length L is depicted in Figure 4. In contrast to the wear of vitrified bonded grinding wheels, metal bonded grinding wheels had a much lower wear rate. A vitrified bonded SiC-grinding wheel at a feed rate of 240 mm/min and a depth of cut of 30 µm showed a profile wear of 30 µm after a grinding length of 2,000 mm (Klocke et al. [10]). A metal bonded tool had a profile wear of just 5 µm for the same process parameters.

The variation of the feed rate between 60 mm/min and 480 mm/min at a constant depth of cut had just a minor influence on the profile wear. This behavior suggests that the mechanical loads, which increase with increasing feed rates, do not affect the tool wear. The tool wear is mainly dependent on the depth of cut. At a grinding length of 1,000 mm, the radial profile wear at a depth of cut of 60 µm is much higher than that for a depth of cut of 30 µm. The increase of the depth of cut raises the contact length between the grinding wheel and the workpiece. A long contact length reduces the supply of lubricant and impedes the removal of chips. The lack of lubricant increases the friction between the grinding wheel and the workpiece. Furthermore, as the chips clog the grinding wheel topography, the grinding effectiveness of the abrasive grains is reduced, thus increasing the thermal loads on the grinding wheel. As a consequence, the thermal loads can increase the profile wear. The supply of lubricant can be improved by using grinding wheels with a larger grain size, but these profiles did not reach the required profile geometries after dressing.

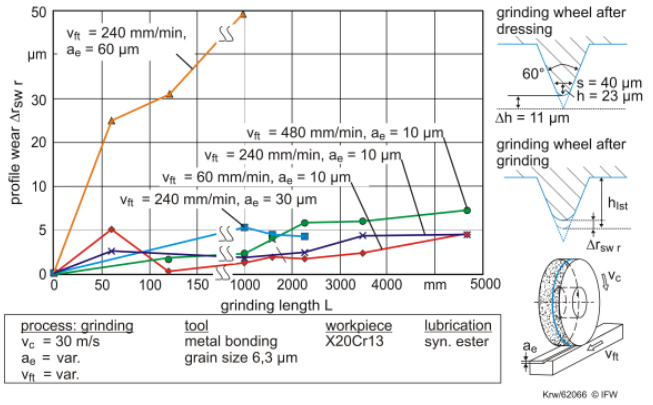

Figure 4. WEAR BEHAVIOR OVER THE GRINDING LENGTH FOR DIFFERENT v_f AND a_e

With the metal bonded grinding wheel grooves were generated with a depth of 7 µm and a width of 17 µm and hence an aspect ratio of $h/s \approx 0.4$. Such an aspect ratio cannot be attained with vitrified bonded grinding wheels. Nevertheless, the wear of metal bonded grinding wheels at a depth of cut of about 60 µm is unacceptably high. Consequently, vitrified and metal bonded grinding wheels have different areas of application. Whereas metal bonded grinding wheels can be used for the manufacturing of small riblet geometries with a riblet height of 10 µm, vitrified bonded grinding wheels should be used for the grinding of riblet structures with a height of more than 30 µm.

RECENT ADVANCES IN MANUFACTURING OF RIBLETS BY LASER-STRUCTURING

As shown in [6], the production of riblets using short pulsed laser radiation in the pulse length regime of several picoseconds yields very good machining results. The flexibility of laser machining is especially valuable since variable riblet spacing can be easily achieved by simple on-the-fly

modification of the machining parameters. A schematic of a laser machining setup is shown in Figure 5.

Using the shown processing method, an area processing rate of 0.1 mm²/s can be achieved. This speed can be increased significantly by using optical components to split the laser beam into multiples without changing the relevant beam characteristics [13]. Therefore, the available laser power can be fully exploited, whereas with a single beam setup the maximum applicable power is limited by the ablation regime, where pulse energies above 7 µJ – 35 µJ cause thermal ablation and insufficient machining results [14]. On modern lasers, pulse energies of 125 µJ are readily available, thus, using an appropriate optical setup, a speed increase up to a factor of 17 is possible depending on the riblet geometry.

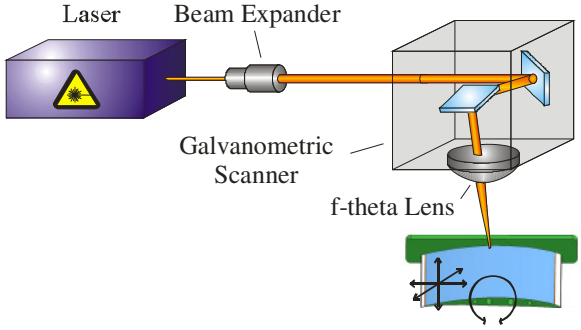

Figure 5. PRINCIPAL SETUP FOR LASER MACHINING. THE MULTI-AXIS TRANSLATION SYSTEM POSITIONS THE AREA OF INTEREST OF THE BLADES INTO THE FOCAL PLANE OF THE LENS, WHILE THE SCANNER DEFLECTS THE LASER BEAM AT HIGH SPEED

Parallel processing is achieved by augmenting the single beam setup by an additional diffractive optical element (DOE) for beam splitting purposes, which is put into the beam between the beam expander and scanner. Since the beam distances in the focal plane are fixed, dynamic rotation of the DOE is used to change the laser spot distance in relation to the scanning direction (Figure 6).

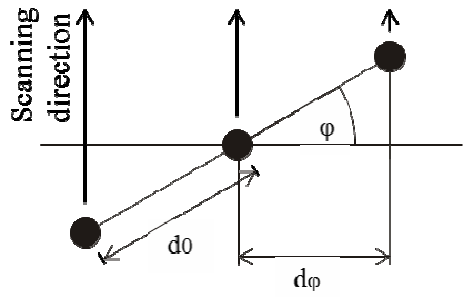

Figure 6. PRINCIPLE OF THREE SPOT ABLATION USING BEAM SPLITTING DOE, THE EFFECTIVE SPOT-TO-SPOT DISTANCE IS DETERMINED BY THE ROTATION ANGLE OF THE DOE

The fan of laser spots created by the DOE enables the parallel machining of riblets along the entire blade length. This is done by scanning hatched rectangles with a width of the spot-to-spot distance and a hatch distance of the riblet width (Figure 7). The point-to-point width for every riblet-geometry has to be matched for an even overall width to avoid curved outlines that would cause non-machined areas [15].

So far, an increase in speed by a factor of five was achieved (0.5 mm²/s vs. 0.1 mm²/s effective scan speed) using a seven spot DOE. An asymptotical closure by a factor of seven seems highly probable using electro optical switches instead of the mechanical ones used in our experimental setup. The ablation quality is equal to single-spot machining and especially improved in parameter transition zones, where sudden breaks are smoothed and bifurcations of lower frequency riblets occur (Figure 8). This brings laser machining of riblets closer to industrial applicability.

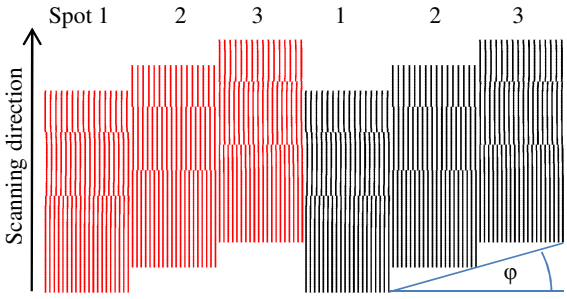

Figure 7. SIMULATED LANE-WISE SCANNING PATTERN USING A 3 SPOT DOE: TWO LANES ARE SET SIDE-BY SIDE USING THREE DIFFERENT RIBLET SPACINGS (FROM TOP TO BOTTOM)

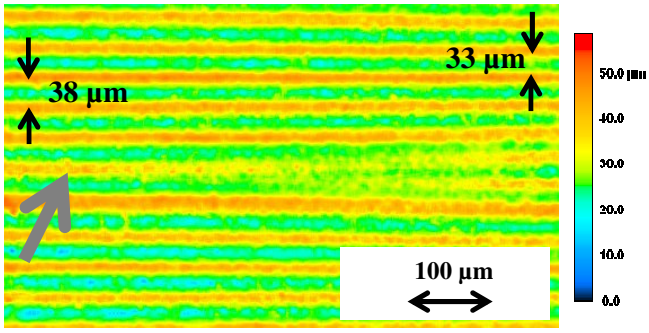

Figure 8. MAGNIFIED CONFOCAL MICROSCOPE IMAGE OF A SMOOTH PARAMETER SET TRANSITION FROM 38 µm TO 33 µm RIBLET SPACINGS. THE GREY ARROW MARKS A BEGINNING BIFURCATION

GEOMETRICAL MEASUREMENT OF RIBLETS

Theory: Physical limitations of the measurement principle

All optical measurement instruments are characterized by the limited lateral resolution which is often defined as

$$d_{\min} = 0{,}61\frac{\lambda}{NA} \qquad (1)$$

with the wavelength λ of the used light. Since the numerical aperture (*NA*) of lenses used in air is less than 1, the lateral resolution is limited to approximately 200 nm. Another problem is the limited capability to detect inclined surfaces. The more a surface is tilted, the less light will be reflected into the measurement lens. After reaching the critical angle (approximately 36°), the signal becomes too degraded for a reliable surface detection. Undetected points are interpolated to counteract this effect, which sometimes leads to inaccurate results.

Limited adaptability of optic methods is demonstrated in Figure 9. The intensity distribution of the cutting line is shown in the two image stacks. In the sample processed with the laser (left), the flank is clearly recognizable due to a rough surface. The foil surface (right), in contrast, hardly gives any signal, therefore only the bottom and the highest points are recognizable.

A µSurf Nanofocus confocal microscope with three objective lenses was used for imaging the riblet structures. The microscope characteristics are summarized in Table 1.

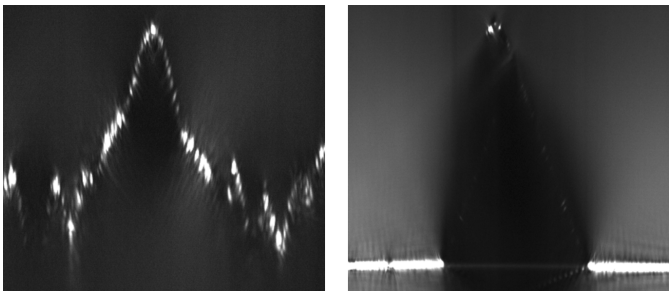

Figure 9. INTENSITY DISTRIBUTION THROUGH THE IMAGE STACK FOR DIFFERENT SAMPLES

Table 1. SYSTEM CHARACTERISTICS OF THE CONFOCAL MICROSCOPE

Magnification	20	50	100
Working distance [mm]	3.1	0.66	0.34
Measurement area [µm^2]	800 · 772	320 · 308.8	160 · 154.4
NA	0.46	0.8	0.95
Max. theoretic slope angle [°]	17.7	26.6	35.5
Lateral resolution [µm]	0.78	0.34	0.2

Choice of measurement lenses

In theory, a lens with 100x magnification is best suited for the measurement. However, 100x lenses have a severe disadvantage: The measurement area is limited to ca. 160 x 160 µm. As the riblets have a typical spacing of 40-80 µm, the measurement only contains 4-2 riblet periods. Such a small area is not suitable for a statistically significant characterization of the riblet-geometry, and therefore has to be enlarged by capturing the surface in small patches. These patches are normally merged by a correlation method (the so called stitching process). Since the stitching of measured data with many surface defects doesn't always work properly, the 100x lens is not the best solution. A smaller magnification has to be chosen to enlarge the captured area. It was determined experimentally that the use of the 20x-lens results in errors in the detection of the tip radii due to poor lateral resolution and the riblet profile was not reproduced accurately due to optical artifacts such as bat-wings. Therefore, the use of the 20x-lens is not recommended for riblet analysis. The 50x lens was chosen because it provides the best compromise between lateral resolution and measurement area even though the measurement results differ from those obtained using the 100x lens, which shows slightly more accurate results because of the higher lateral resolution. This effect is also depicted in the histograms (Figure 13).

Interpolation of surface defects

Due to the steep flank angle of the riblet structures, the information in the area of the flanks must be estimated by interpolation. Typically, bilinear interpolation is utilized, but investigations of nearly ideal riblet structures (especially when using lenses with 50x and 100x magnification) indicated that bilinear interpolation results in a significantly inaccurate indication of surface deformation (Figure 10). Hence, the triangle-based cubic interpolation was used instead of the bilinear interpolation. The basic triangles are defined with the help of Delaunay triangulation. A result of the interpolation is depicted in Figure 10.

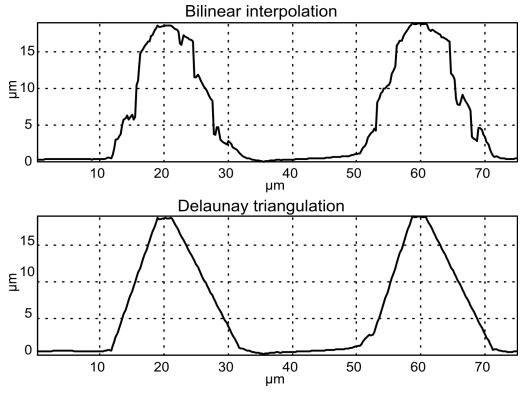

Figure 10. RESULTS OF BILINEAR INTERPOLATION (TOP) AND INTERPOLATION BASED ON DELAUNAY TRIANGULATION

Calculation of main parameters

The aerodynamic performance of the riblets is a function of their spacing, height and tip radius. These parameters are measured using the following methodology.

Riblet spacing and height:

The spacing of the riblets produced by grinding and laser-structuring varies over the surface. In order to define this variation, the calculation of the riblet spacing is performed locally over a small region within the overall measured area. This region is moved along the whole surface, and at each position, the significant parameters are calculated as shown in step two.

1. **Region pre-processing:** The region described in step 1 has to be large enough to contain at least two complete riblet periods. Since the riblets are periodic structures, they can be approximated with dominant and harmonic waves using Fast-Fourier-Transformation (FFT). In order to obtain correct results from the FFT, the examined region has to contain whole-numbered amounts of riblet waves. If the requirements are not met, the so-called leakage effect will occur and the structures are approximated by waves of incorrect frequencies. Because the period length is not known a priori, this condition is not met generally, and therefore the region will be cut out using zero-padding technique (Vynnyk [16]).
2. **Region analysis:** The following steps are performed after pre-processing the selected region as described in step 1:
    a. FFT for pre-processed region.
    b. Simplification of the spectrum (all frequencies except the dominant wave and their three harmonics are set to zero).
    c. Inverse FFT.

    A result of such "simplification" of a complex manufactured surface structure is shown in Figure 11.

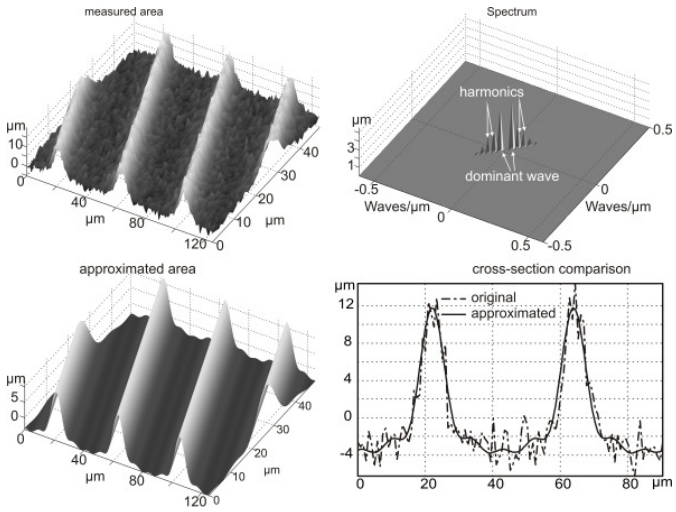

Figure 11. ELIMINATION OF THE STOCHASTIC PARTS

Tip Radii:

Contrary to the spacing and height of the riblets, the tip radii are not integral characteristics, but describe a local behavior of the surface. Therefore, the FFT cannot be applied to evaluate the tip radii and the following steps should be performed:

1. One period is extracted using the region analysis.
2. The upper 5% of the profile data is cut off from the rest. This data describes the actual tip area of the riblet as shown in Figure 12.
3. A 3rd order polynomial fit is performed from which the peak point is obtained.
4. If the radius of curvature at the peak of the 3rd order polynomial fit obtained in step 3 is less than the width of the 5% "profile tip" obtained in step 2, it is assumed to be the riblet tip radius.

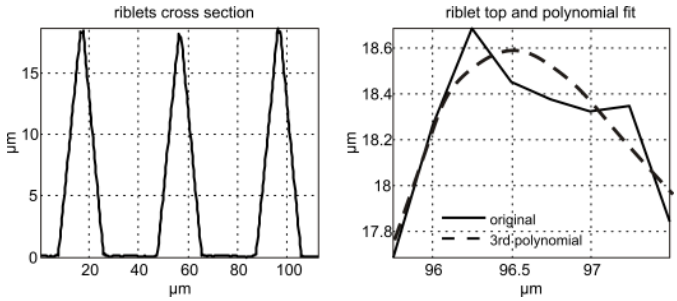

Figure 12. DEFINITION OF THE TOP AREA

Verification of the tip radii with the SEM

As shown in the histograms (Figure 13), the calculated tip radii depend on the lens used for making the measurements. In order to clear the impreciseness, a scanning electron microscope (DSM 940A) with a 2 detector system and an image–acquisition unit from Point Electronics was used to verify the riblet tip radii.

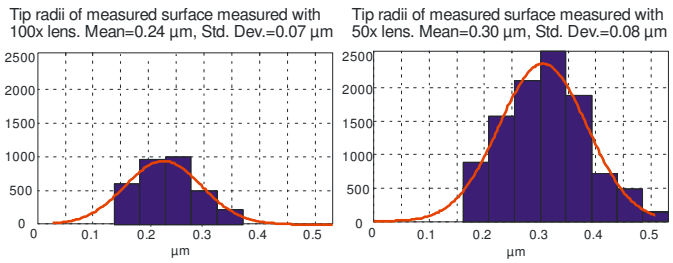

Figure 13: DIFFERENT MEASURMENT RESULTS OF THE SAME SPECIMEN

A typical SEM-picture of a foil sample is shown in Figure 14. The bright areas represent the riblet flanks, whereas the dark areas denote the horizontal areas. A cut through the picture gives a profile as seen in Figure 14.

The tip width can be considered to be the distance between the highest negative and positive inclination of the intensity distribution. The flank angle should also be accounted for in the calculation of the tip radius. However, in order to maintain compatibility with the optical measured data, the influence of the flank angle is neglected and the tip radius is defined as follows:

$$r = t/2 \tag{2}$$

The SEM measurements of the tip radius correspond to the measurements made with the confocal microscope and the 50x magnification lens within 20% in all cases.

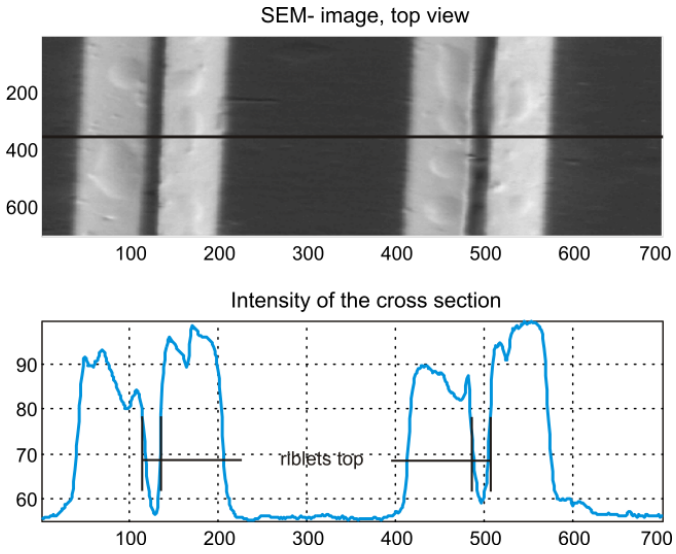

Figure 14. EVALUATION OF RIBLETS RADII USING SEM

AERODYNAMIC MEASUREMENTS

Wall shear-stress reduction

Investigations to validate the aerodynamic effectiveness of ribs manufactured by grinding and laser-structuring were carried out under ideal flow conditions in the oil channel at the Institute of Propulsion Technology of the DLR in Berlin. The main advantage of these investigations, in contrast to the investigations conducted on compressor blades in the linear cascade wind tunnel, is that the effect of the surface structures on skin friction was determined under the simplest flow conditions, using flat plates with the riblets perfectly aligned with the main flow direction under a zero pressure gradient. Prior to the investigations in the oil channel, ribs were manufactured by grinding and laser-structuring on X20Cr13 probe material in small scales, comparable to the size of the ribs suitable for application on compressor blades. Subsequently, the geometry of the manufactured microstructures was measured using the optical measuring techniques described above. After post-processing the measured data, the surface structures were scaled up to maintain Reynolds similarity for the measurements in oil. The scaled up riblet geometries were generated on the flat plates by rapid prototyping as described in Oehlert at al. [6]. More information on the oil channel test facility and the measurement setup is given in Bechert et al. [4].

Experimental results showing the influence of ground and laser-structured ribs on the relative change of wall shear-stress $\Delta\tau/\tau_0$ as a function of the dimensionless riblet-spacing s^+ in comparison to riblets with an ideal trapezoidal and triangular groove geometry obtained by Bechert et al. [4] are given in Figure 15. The chosen target riblet geometry, characterized by a trapezoidal groove with a flank opening-angle at the tip of $\alpha = 30°$ and a riblet height to spacing ratio of $h/s = 0.5$, is compared to the ground and laser-structured ribs of the present investigation in Figure 16. The geometrical parameters in the evaluation of the aerodynamic effectiveness of the riblets are given in Table 2. In addition to h/s and the ratio of riblet tip-diameter to riblet spacing t/s, a shape factor X is introduced to describe the triangular or the trapezoidal similarity of the groove:

$$X = \frac{A - A_{triangular}}{A_{trapezoidal} - A_{triangular}} \tag{3}$$

For $X = 0$, the shape of the groove is an ideal triangle. For $X = 1$ the groove has an ideal trapezoidal shape. The shape factor is calculated by the IMR during the post-processing of the optical measurement data.

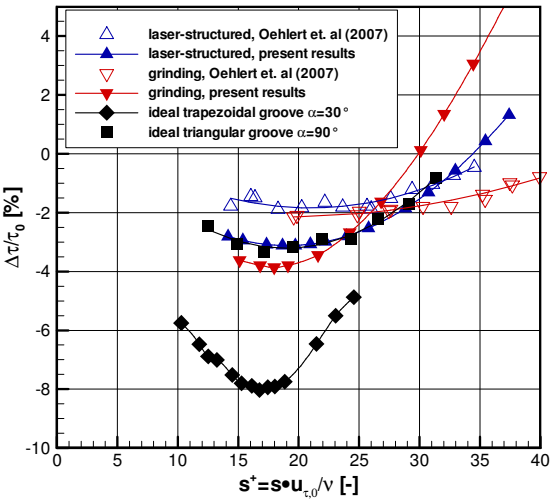

Figure 15. WALL SHEAR-STRESS REDUCTION OF GROUND AND LASER-STRUCTURED RIBLETS IN COMPARISON TO RIBLETS WITH AN IDEAL SHAPE (EXPERIMENTAL DATA MEASURED BY THE GERMAN AEROSPACE CENTER, INSTITUTE OF PROPULSION TECHNOLOGY, ENGINE ACOUSTICS DEPARTMENT); CURVES OBTAINED BY POLYNOMIAL INTERPOLATION; σ=±0.3%

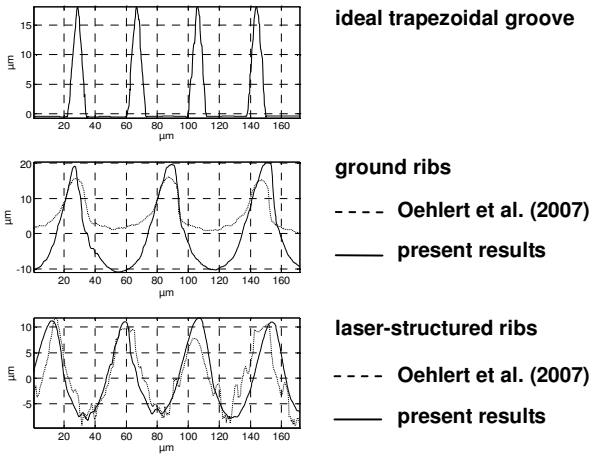

Figure 16. REPRESENTATIVE CROSS SECTIONS OF GROUND AND LASER-STRUCTURED RIBLETS IN COMPARISON TO THE IDEAL GEOMETRY WITH A TRAPEZOIDAL GROOVE

An additional increase of wall shear-stress reduction of $\Delta\tau/\tau_0 = -1\%$ is the result of improvements in the manufacturing techniques as is demonstrated by a comparison of the data presented by Oehlert et al. [6] with the result of the present investigations in Figure 15. According to Table 2, this enhancement is primarily due to a nearly optimal *h/s* of the ground ribs and an increasingly sharp riblet tip. For the laser-structured ribs, this enhancement can be related to the more trapezoidal groove geometry. Further improvements towards reducing skin friction can thus be achieved by an additional decrease of the tip diameter and a more trapezoidal shape of the groove geometry to even further dampen the cross flow of the streak structures at the wall.

Table 2. GEOMETRIC PARAMETERS OF GROUND AND LASER-STRUCTURED RIBS

riblets	*h/s* [-]	*t/s* [-]	*X* [%]
laser-structured, Oehlert et al. (2007)	0.39	0.04	10.2
laser-structured, present results	0.39	0.04	32.5
grinding, Oehlert et al. (2007)	0.25	0.04	51.4
grinding, present results	0.49	0.02	53.1

Calculation of wall shear-stress reduction

An empirical model was developed to investigate the potential for the optimization of the grinding and laser-structuring processes. The model enables the calculation of the wall shear-stress reduction $\Delta\tau/\tau_0$ of riblets as a function of the geometrical riblet-parameters spacing *s*, height *h*, tip-radius *r* and shape factor *X*. The model was derived by a regression analysis of the oil channel data obtained for ideal riblets by Bechert et al. [4] and Hage and Bechert [17], as well as various riblets produced by grinding and laser-structuring.

Exemplary comparisons between calculated and measured wall shear-stress reduction $\Delta\tau/\tau_0$ as a function of the dimensionless riblet spacing s^+ for ideal structures and for ground and laser-structured riblets are given in Figure 17 and Figure 18.

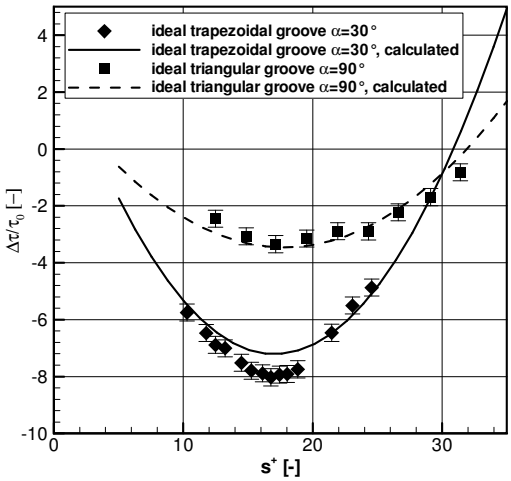

Figure 17. COMPARISON OF MEASURED AND CALCULATED WALL SHEAR-STRESS REDUCTION FOR IDEAL RIBLETS; ERROR BARS INDICATE THE STANDARD DEVIATION σ

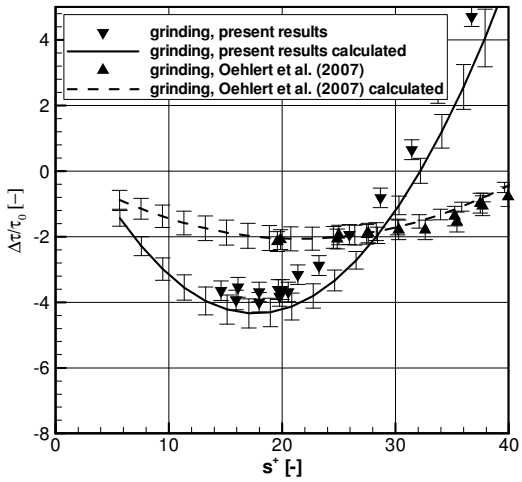

Figure 18. COMPARISON OF MEASURED AND CALCULATED WALL SHEAR-STRESS REDUCTION FOR GROUND AND LASER-STRUCTURED RIBLETS; ERROR BARS INDICATE THE STANDARD DEVIATION σ

In order to take into account the stochastic distributions of the ground and laser-structured ribs, probabilistic simulations were carried out using a Monte-Carlo Simulation (MCS). A Latin Hypercube Sampling (LHS) was applied to take random samples from the probability density functions of the rib

geometry parameters as depicted in Figure 19. Overall, N=2000 samples were taken for the MCS. It was determined in preliminary investigations that the mean values and standard deviations of the results are independent of the sample number for N=2000. Extensive calculations to validate the model, which are not shown here, were conducted on different rib-structures produced by grinding and laser-structuring. Overall, the experimental and calculated wall shear-stress reduction corresponds well and the validation process showed that the physical effects of the geometry parameters on wall shear-stress are well captured by the model.

Probabilistic calculations on compressor blades

Numerical calculations on riblet-structured NACA 6510 compressor blades were performed using MISES, which is a viscous-inviscid cascade analysis and design system. A brief overview of the cascade flow solution method used in MISES is given by Drela and Giles [18]. MISES was modified and validated in order to account for the drag-influencing effects of ideal trapezoidal groove riblets by Lietmeyer et al. [19]. To evaluate the drag-influencing effects of ground and laser-structured riblets, the model of shear-stress reduction as an empirical function of the riblet-geometry described above was implemented in MISES.

Numerical simulations using MISES embedded in a Monte-Carlo Simulation were performed in order to calculate the profile-loss reduction of a blade structured by grinding. The goal of the simulations was to define further improvements in the structuring process. For the Latin Hypercube Sampling, the probability density functions of the geometrical parameters of the surface structure were taken into account as shown in Figure 19. The blade was structured only on the suction side in the turbulent boundary layer downstream of a dimensionless chord length of $x/c = 0.4$. Overall, N=2000 simulations were conducted using MISES. For each simulation run, the pressure loss coefficient was calculated:

$$\omega = \frac{p_{tot,1} - p_{tot,2}}{p_{tot,1} - p_{stat,1}} \tag{4}$$

To determine the effect of the riblets on the pressure loss, the difference in the loss coefficient was calculated:

$$\frac{\Delta\omega}{\omega_0} = \frac{\omega - \omega_0}{\omega_0} \tag{5}$$

In Eq. (5) ω is the loss coefficient of the riblet-structured blade and ω_0 is the loss coefficient of the smooth reference blade. The cascade inlet flow conditions are M=0.5 and Re=10^6. Further information on the experimental setup and blade specifications is given in [9].

As a result of the MCS with MISES, a mean profile-loss reduction of $\Delta\omega/\omega_0 = -1.89\% \pm 0.42\%$ was calculated for the current blade structured by grinding and is in good accordance with the experimental result of $\Delta\omega/\omega_0 = -1.38\% \pm 0.29\%$. Additional conclusions from the numerical results can be drawn by plotting the profile-loss reduction ω/ω_0 over each individual realization of the MCS as depicted in Figure 20. By applying a correlation analysis of the data, Pearson's correlation coefficient was calculated. Results of the correlation analysis are plotted in a PIE-chart by normalizing each correlation coefficient by the total sum (Figure 21). With the help of this analysis it becomes obvious that an additional reduction of profile-loss can be achieved by decreasing the riblet tip-diameter and by a more trapezoidal shaped groove. This supports the experimental results obtained in the oil channel presented above.

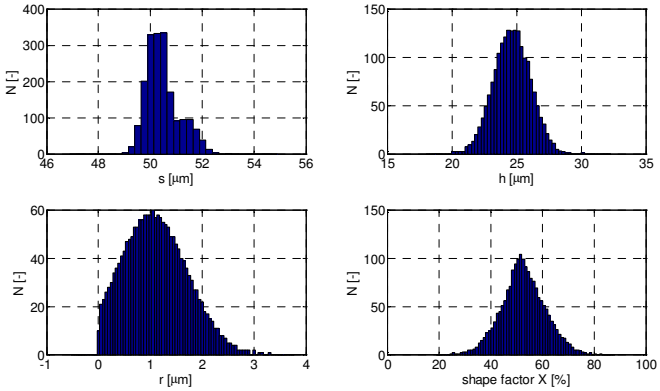

Figure 19. PROBABILITY DENSITY FUNCTIONS OF GEOMETRIC PARAMETERS OF A GROUND RIBLET STRUCTURE ON A NACA 6510 COMPRESSOR BLADE (MEASURED BY IMR)

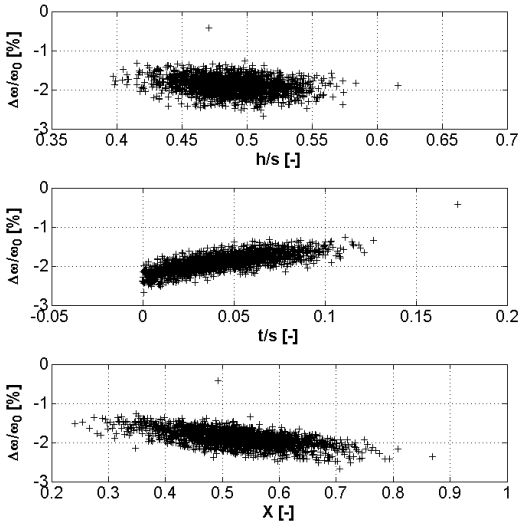

Figure 20. ANT-HILL-PLOTS OF PROFILE-LOSS REDUCTION

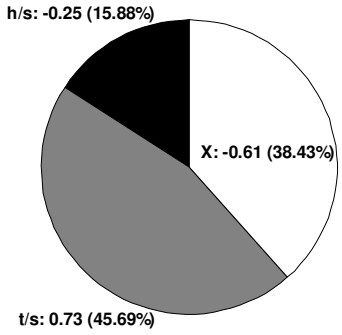

Figure 21. PIE-CHART OF PROFILE-LOSS REDUCTION

CONCLUSIONS

Recent advances in the manufacturing of riblets by grinding and laser-structuring in relation to the geometric quality of the ribs and their aerodynamic effectiveness are presented.

Grinding with multi-profiled grinding wheels is an effective method for generating riblets on large-scale surfaces. With vitrified bonded grinding wheels, a reproducible aspect ratio of riblet height to spacing of $h/s = 0.5$ is presently only achievable for a riblet spacing of $s > 60$ µm. This is the optimal aspect ratio for attaining the maximum reduction of skin friction for riblets with a trapezoidal groove, which is the target geometry. However, especially near the leading edge of compressor blades under turbomachinery-like flow conditions, the desired riblet spacing is $s < 60$ µm with a minimum of $s \approx 20$ µm. To achieve the aspect ratio of h/s=0.5 for such small riblet spacings, metal bonded grinding wheels were applied due to their smaller grain size. With metal bonded grinding wheels, riblets with a spacing of $s > 17$ µm and an aspect ratio of $h/s = 0.4$ were achieved, which is a significant improvement compared to vitrified bonded grinding wheels. A promising result is a reduction in the wear of metal bonded grinding wheels to 1/6 of the wear of vitrified bonded grinding wheels for a cut depth smaller than 30 µm. For a cut depth greater than 30 µm, the wear of metal bonded grinding wheels significantly increases. This leads to the conclusion that grinding wheels with a metal bonding are particularly suitable for the manufacturing of small riblet geometries with a riblet height of 10 to 30 µm. Vitrified bonded grinding wheels should be applied for the grinding of riblet structures with a riblet height of more than 30 µm.

For the laser-structuring process, a significant decrease of production time was achieved by applying diffractive optical elements. Presently, an increase in speed by a factor of five has been achieved using a seven-spot DOE. The variation of the rotation angle of the DOE during the manufacturing process provides the opportunity for a continuously adaption of the riblet geometry along the blades's surface to the local flow conditions.

To characterize the aerodynamic impact of the riblets manufactured by grinding and laser-structuring, the surface structures were measured with a confocal microscope and 50 times magnification. The measured values were confirmed with a Scanning Electron Microscope. The structured surface was measured in small patches which were stitched together in the post-processing. Probability density functions of riblet spacing and height were calculated by an FFT. The probability density function of the riblet tip-diameter was calculated by means of a 3rd order polynomial approximation.

For both ground and laser-structured ribs, an additional reduction of wall shear-stress by approximately $\Delta\tau/\tau_0 = -1\%$ was obtained due to improvements in the manufacturing techniques, which presently leads to a maximum reduction in skin friction of $(\Delta\tau/\tau_0)_{max} \approx -4\%$. For the ground ribs, this enhancement is shown to be primarily due to a nearly optimal riblet height-to-spacing ratio and sharper riblet tips. For the laser-structured ribs, this enhancement can be related to the more trapezoidal groove geometry. A further reduction of skin friction could thus be achieved by a further decrease of the tip diameter and a more trapezoidal shape of the groove geometry.

To assess the impact on compressor blade profile losses and in order to indentify the potential for future optimization of the grinding and laser-structuring processes, an empirical model of wall shear-stress reduction as a function of the relevant riblet geometry parameters was developed. The empirical model was implemented in the viscous-inviscid cascade analysis code MISES. This combination delivers a design tool to calculate profile losses of riblet-structured linear blade cascades. Numerical simulations with MISES embedded in a Monte-Carlo-Simulation (MCS) were performed in order to calculate the profile-loss reduction of a compressor blade structured by grinding. As a result of the MCS with MISES, a mean profile-loss reduction of $\Delta\omega/\omega_0 = -1.89\% \pm 0.42\%$ was calculated and is in good accordance with the experimental result of $\Delta\omega/\omega_0 = -1.38\% \pm 0.29\%$. By applying a correlation analysis of the data obtained by the MCS and a calculation of Pearson's correlation coefficient, it was confirmed that an additional reduction of profile loss of up to 4% for the investigated NACA 6510 compressor cascade can be achieved by decreasing the riblet tip-diameter further and by a more trapezoidal shaped groove. This loss reduction was measured by [9] on the compressor cascade carrying a riblet foil on the suction side with an ideal trapezoidal groove geometry.

ACKNOWLEDGMENTS

The research of this paper is based on a cooperation between the Institute for Turbomachinery and Fluid Dynamics (TFD), the Institute for Measurement and Automatic Control (IMR), the Institute of Production Engineering and Machine Tools (IFW), all of Leibniz Universität Hannover and the Laser-Center Hannover (LZH). The joint research project was sponsored by the DFG (Deutsche Forschungsgemeinschaft) under Grants PAK 182, GZ SE 1023/13-3.

Many thanks go to our former project partners Wolfram Hage and Robert Meyer of the Institute of Propulsion

Technology of the German Aerospace Center in Berlin, who provided the data of the oil channel measurements. Additionally, the authors are very grateful to all the comments of the anonymous reviewers which led to a significant improvement of the paper.

REFERENCES

[1] Gümmer, V., (2005), "Pfeilung und V-Stellung zur Beeinflussung der dreidimensionalen Strömung in Leiträdern transsonischer Axialverdichter," Fortschritt-Berichte VDI Reihe 7 Nr. 384, VDI Verlag, Düsseldorf

[2] Reif, W.-E., 1985, "Squamation and ecology of sharks," Courier Forschungsinstitut Senckenberg, Frankfurt/Main, 78, ISBN 0341-4116

[3] Walsh, M. J., 1983, "Turbulent boundary layer drag reduction using riblets," AIAA paper 82-0169

[4] Bechert, D. W., Bruse, M.; Hage, W., van der Hoeven, J. G. T. and Hoppe, G., 1997, "Experiments on drag-reducingsurfaces and their optimization with an adjustable geometry," *Journal of Fluid Mechanics*, **338**, pp. 59-87

[5] Oehlert, K. and Seume, J., 2006, "Exploratory experiments on machined riblets on compressor blades," *Proc. of FEDSM 2006*, Miami, FL, USA, FEDSM 2006 – 98093

[6] Oehlert, K., Seume J., Siegel F., Ostendorf, A., Wang, B.; Denkena, B., Vynnyk, T., Reithmeier, E., Hage, W., Knobloch, K. and Meyer, R., 2007, "Exploratory experiments on machined riblets for 2-D compressor blades," *Proc. of IMECE2007*, Seattle, Washington, USA, IMECE 2007 – 43457

[7] Denkena, B., Koehler, J. and Wang, B., 2010, "Manufacturing of functional riblet structures by profile grinding," *CIRP Journal of Manufacturing Science and Technology*, **3**, pp. 14-26

[8] Siegel, F., Klug, U. and Kling, R., 2009, "Extensive Micro-Structuring of Metals using Picosecond Pulses – Ablation Behavior and Industrial Relevance," *JLMN-Journal of Laser Micro/Nanoengineering*, **4**, pp. 104-110

[9] Lietmeyer, C., Oehlert, K. and Seume J. R., 2011, "Optimal application of riblets on compressor blades and their contamination behaviour," *Proc. of ASME Turbo Expo 2011*, Vancouver, Canada, GT2011-46855

[10] Klocke, F., Klink, A. and Schneider, U, 2007, "Electrochemical oxidation analysis for dressing bronze-bonded diamond grinding wheels," *Production Engineering - Research and Development (WGP)*, **1**, Number 2, pp. 141-148

[11] Denkena, B., Reichstein, M. and Hahmann, D., 2006, "Electro Contact Discharge Dressing for Micro-Grinding," *Proceedings of the 6th euspen International Conference*, Baden, Austria, pp. 92 - 956

[12] Zaeh, M.F., Brinksmeier, E., Heinzel, C., Huntemann, J.W. and Föckerer, T, 2009, "Experimental and numerical identification of process parameters of grind-hardening and resulting part distortions," *Production Engineering - Research and Development (WGP)*, **3**, Number 3, pp. 271-279

[13] Golub, M., 2004, "Laser Beam Splitting by Diffractive Optics," *Optics and Photonics News*, **15**, Issue2

[14] Siegel, F., 2011, "Abtragen metallischer Werkstoffe mit Pikosekunden-Laserpulsen für Anwendungen in der Strömungsmechanik," Dissertation, Berichte aus dem LZH, Band 02/2011

[15] Wojakowski, B., Klug, U. and Kling, R., 2011, "Large-Area Production of Dynamically Scaled Micrustructures using Diffractive Optical Elements," *Proc. of ICALEO 2011*, Orlando Florida, M603

[16] Vynnyk, T., 2010, "REM-Topografiemessungen an mikro- und nanostrukturierten Oberflächen," Dissertation, Leibniz Universität Hannover

[17] Hage, W. and Bechert, D.W., 2001, "Rib tip sharpness: a key issue for riblet application," Interner Bericht, DLR-IB 92517-01/B7

[18] Drela, M. and Giles, M.B., 1987, "Viscous-Inviscid Analysis of Transonic and Low Reynolds Number Airfoils," *AIAA Journal*, **25**, No. 10, pp. 1347-1355

[19] Lietmeyer, C., Chahine, C. and Seume, J.R., 2011, "Numerical Calculation of the Riblet-Effect on Compressor Blades and Validation with Experimental Results," *Proc. of IGTC 2011*, Osaka, Japan, IGTC2011-0106

